BRAIN COMMUNICATIONS

Magnetic resonance imaging biomarkers of cerebrospinal fluid tracer dynamics in idiopathic normal pressure hydrocephalus

Per Kristian Eide,[1,2] Are H. Pripp[3] and Geir Ringstad[4]

Disturbed clearance of toxic metabolites from the brain via cerebrospinal fluid is emerging as an important mechanism behind dementia and neurodegeneration. To this end, magnetic resonance imaging work-up of dementia diseases is largely focused on anatomical derangements of the brain. This study explores magnetic resonance imaging biomarkers of cerebrospinal fluid tracer dynamics in patients with the dementia subtype idiopathic normal pressure hydrocephalus and a cohort of reference subjects. All study participants underwent multi-phase magnetic resonance imaging up to 48 h after intrathecal administration of the contrast agent gadobutrol (0.5 ml, 1 mmol/ml), serving as cerebrospinal fluid tracer. Imaging biomarkers of cerebrospinal fluid tracer dynamics (i.e. ventricular reflux grades 0–4 and clearance) were compared with anatomical magnetic resonance imaging biomarkers of cerebrospinal fluid space anatomy (Evans' index, callosal angle and disproportional enlargement of subarachnoid spaces hydrocephalus) and neurodegeneration (Schelten's medial temporal atrophy scores, Fazeka's scores and entorhinal cortex thickness). The imaging scores were also related to a pulsatile intracranial pressure score indicative of intracranial compliance. In shunt-responsive idiopathic normal pressure hydrocephalus, the imaging biomarkers demonstrated significantly altered cerebrospinal fluid tracer dynamics (ventricular reflux grades 3–4 and reduced clearance of tracer), deranged cerebrospinal fluid space anatomy and pronounced neurodegeneration. The altered MRI biomarkers were accompanied by pressure indices of impaired intracranial compliance. In conclusion, we present novel magnetic resonance imaging biomarkers characterizing idiopathic normal pressure hydrocephalus pathophysiology, namely measures of cerebrospinal fluid molecular redistribution and clearance, which add information to traditional imaging scores of cerebrospinal fluid space anatomy and neurodegeneration.

1 Department of Neurosurgery, Oslo University Hospital-Rikshospitalet, Oslo, Norway
2 Institute of Clinical Medicine, Faculty of Medicine, University of Oslo, Oslo, Norway
3 Oslo Centre of Biostatistics and Epidemiology, Oslo University Hospital, Oslo, Norway
4 Department of Radiology, Oslo University Hospital- Rikshospitalet, Oslo, Norway

Correspondence to: Professor Per Kristian Eide, MD PhD,
Department of Neurosurgery,
Oslo University Hospital – Rikshospitalet,
PB 4950 Nydalen, 0424 OSLO, Norway,
E-mail: p.k.eide@medisin.uio.no

Keywords: idiopathic normal pressure hydrocephalus; MRI biomarkers; ICP; cerebrospinal fluid; glymphatic system

Abbreviations: BBB = blood–brain barrier; CSF = cerebrospinal fluid; DESH = disproportional enlarged subarachnoid space hydrocephalus;ERC = entorhinal cortex; gMRI = glymphatic magnetic resonance imaging; ICP = intracranial pressure; iNPH = idiopathic normal pressure hydrocephalus; MTA = medial temporal atrophy; MWA = mean ICP wave amplitude; REF = reference patient; ROC = receiver operating characteristics; ROI = region of interest

Received June 13, 2020. Revised September 09, 2020. Accepted September 22, 2020. Advance Access publication November 2, 2020

Graphical Abstract

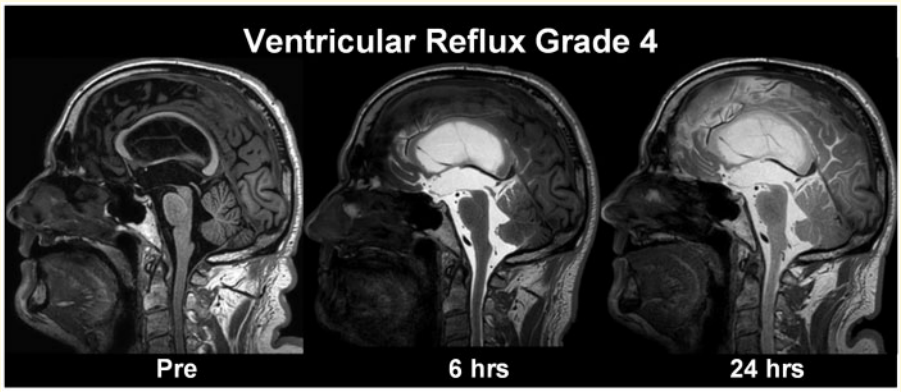

Introduction

Idiopathic normal pressure hydrocephalus (iNPH) is a neurological disease characterized clinically by gait disturbance, urinary incontinence and dementia, with imaging findings of enlarged ventricles, and cerebrospinal fluid (CSF) pressure within normal range (Relkin *et al.*, 2005). The disease is a subtype of dementia with resemblances to Alzheimer's disease (Leinonen *et al.*, 2010; Cabral *et al.*, 2011; Pomeraniec *et al.*, 2016). Both diseases show deposition of toxic metabolites such as amyloid-β and tau in brain tissue, and histological specimens from cortical biopsies reveal an overlap with Alzheimer's disease in about one-third to half of the iNPH patients (Leinonen *et al.*, 2010; Libard and Alafuzoff, 2019). Tau lacks blood–brain barrier (BBB) transporters, and clearance of some toxic isoforms of amyloid-β (e.g. pyroglutamate Aβ, pE3-Aβ) also depends on removal along extravascular pathways (Jawhar *et al.*, 2011). Since the subarachnoid CSF compartment is continuous with the brain interstitial compartment via perivascular spaces (Iliff *et al.*, 2012; Ringstad *et al.*, 2018), molecular clearance failure from CSF may thus be crucial for the accumulation of toxic metabolites in iNPH as well as Alzheimer's disease (Reeves *et al.*, 2020).

Currently, there is a major interest in the role of meningeal lymphatic CSF drainage for cerebral waste removal in age-related cognitive decline and Alzheimer's disease evolvement (Ma *et al.*, 2017; Da Mesquita *et al.*, 2018; Zhou *et al.*, 2020). Experimental studies in animals provide evidence that clearance of neurotoxic metabolites from CSF is hampered by defective meningeal lymphatic clearance mechanisms (Louveau *et al.*, 2017). Lately, *in vivo* studies in humans have shown that a CSF tracer contained outside the BBB drains to parasagittal dura (Ringstad and Eide, 2020), and to extra-cranial lymph nodes (Eide *et al.*, 2018). The efficacy of meningeal lymphatic drainage declines with age (Zhou *et al.*, 2020). However, the clinical implications remain unclear, not least the role of imaging of molecular clearance failure.

In several respects, the iNPH disease is a model of other dementia types such as Alzheimer's disease (Libard and Alafuzoff, 2019), as illustrated by cerebral amyloid-β/tau deposition (Leinonen *et al.*, 2010), signs of neurodegeneration (Libard and Alafuzoff, 2019), loss of BBB integrity (Eide and Hansson, 2020), and evidence of CSF molecular clearance failure (Ringstad *et al.*, 2017). To study these mechanisms in iNPH, we have utilized multiphase magnetic resonance imaging (MRI) with an intrathecal contrast agent as CSF tracer (Ringstad *et al.*, 2017; Eide and Ringstad, 2019). Establishing MRI biomarkers indicative of impaired CSF molecular distribution and clearance might even be of value for other dementia diseases beyond iNPH.

In contrast to other types of dementia, iNPH may be treated and improved by CSF shunt surgery (Eide and Sorteberg, 2016). Since shunt surgery has a definite risk, various invasive tests are used to identify the iNPH patients who most likely will respond to shunt surgery, and to rule out those who will not (Marmarou *et al.*, 2005). Ancillary tests include temporary lumbar drainage of CSF, lumbar infusion tests, and overnight monitoring of intracranial pressure (ICP) (Marmarou *et al.*, 2005). In our practice, the finding of elevated ICP wave amplitudes, which is indicative of impaired intracranial compliance (or reduced ICP–volume reserve capacity), has been used with high accuracy in identifying iNPH responders (Eide and Sorteberg, 2010, 2016). However, the development of less invasive methods based on imaging alone is desirable.

The present study was undertaken to assess how MRI biomarkers of CSF tracer dynamics (CSF tracer ventricular redistribution and molecular clearance) compare with other conventional MRI biomarkers of CSF space anatomy and neurodegeneration. We also examined how the MRI biomarkers differentiated shunt-responsive iNPH patients from a cohort of reference (REF) subjects. In addition, we examined how the MRI biomarkers associated with a pulsatile ICP score indicative of the intracranial compliance.

Materials and methods

This observational study was approved by the Regional Committee for Medical and Health Research Ethics (REK) of Health Region South-East, Norway (2015/96), the Institutional Review Board of Oslo university hospital (2015/1868), and the National Medicines Agency (15/04932-7). The study was conducted governed by ethical standards according to the Helsinki Declaration of 1975 (and as revised in 1983). Study participants were included after written and oral informed consent.

Experimental design

The primary objective of the present study was to compare structurally and dynamically derived MRI biomarkers of iNPH disease. Secondarily, we examined how the various MRI biomarkers differentiated iNPH patients responding to shunt-surgery ('Definite iNPH') from REF subjects. We also specifically addressed how the MRI biomarkers associated with a pulsatile ICP metric, the mean ICP wave amplitude (MWA), which is indicative of the ICP–volume reserve capacity, i.e., the intracranial compliance (Eide, 2016).

The patients underwent repetitive magnetic resonance imaging (MRI) before/after intrathecal administration of the MRI contrast agent gadobutrol (0.5 mmol); referred to as 'gMRI' (glymphatic magnetic resonance imaging), as it was initially developed to study the human glymphatic system.

We compared three categories of MRI biomarkers, namely MRI biomarkers of (i) CSF tracer dynamics, (ii) CSF space anatomy and (iii) neurodegeneration (see MRI biomarkers section). The predefined set of MRI biomarkers was assessed by a neuroradiologist (G.R.) with 14 years' experience in neuroradiology, and who were blinded to the diagnoses of the patients, as well as to the MWA scores.

Patients

The study includes consecutive patients retrieved from a larger cohort of patients undergoing gMRI as part of their neurosurgical work-up of various CSF disorders within the Department of Neurosurgery at Oslo University Hospital, Norway. The two patient cohorts were included according to the following criteria:

Definite iNPH

The iNPH patients exclusively included patients who were shunted and thereafter improved clinically. We did not include iNPH patients not found eligible for shunting and who were managed conservatively without shunt surgery. The included iNPH patients fulfilled the criteria of 'probable' iNPH according to the American-European guidelines (Relkin *et al.*, 2005). They also fulfilled the criteria of Definite iNPH according to the Japanese guidelines (Mori *et al.*, 2012), i.e., they were clinical responders to shunt surgery.

With regard to clinical improvement after shunting, we have previously described an NPH scoring of symptom severity (15 possible scores ranging from worst 3 to best 15 scores) assesses the combined severity of gait disturbance, urinary incontinence and dementia (Eide and Sorteberg, 2010; Eide and Sorteberg, 2016). Clinical response to shunting was defined as an improvement by at least one score in one or more of the symptoms of gait disturbance, urinary incontinence and cognitive function.

Reference subjects

The REF subjects were individuals who had undergone gMRI for work-up of tentative CSF disturbance, including suspicion of CSF leak, symptomatic cysts and idiopathic intracranial hypertension, but without any objective sign of CSF failure at gMRI, ICP or clinical examination. In none of these were there indications for surgery or other interventions. We included those subjects from the entire REF cohort closest in age with iNPH; and no individuals < 35 years of age were included.

Magnetic resonance imaging biomarkers

The MRI protocol followed a strict and standardized protocol, as previously described (Ringstad *et al.*, 2017; Ringstad *et al.*, 2018). Sagittal 3D T1-weighted gradient echo volume scans were obtained using a 3 T Philips Ingenia MRI scanner (Philips Medical systems, Best, The Netherlands) with equal imaging protocol settings before and at several time points up to 48 h after intrathecal injection of gadobutrol (0.5 mmol). We categorized the MRI exams into the following time intervals based on time interval before/after intrathecal injection. Before intrathecal contrast (Pre), and 40–60 min, 2–4 h, 6–9 h, 24 h and 48 h after intrathecal injection, respectively.

Magnetic resonance imaging biomarkers of CSF tracer dynamics

(a) Ventricular reflux of CSF tracer as a marker of CSF redistribution. The ventricular reflux was assessed using T1-weighted images, and the degree of ventricular reflux was categorized as follows: Grade 0: No supra-aqueductal reflux. Grade 1: Sign of supra-aqueductal reflux. Grade 2: Transient enrichment of lateral ventricles Day 1. Grade 3: Lasting enrichment of lateral ventricles Day 2 (but not isointense with subarachnoid CSF). Grade 4: Lasting enrichment of lateral ventricles Day 2 (isointense with subarachnoid CSF). Assessment Day 1 was done 6 h after MR contrast agent administration, and examination Day 2 was done after about 24 h. The different categories of ventricular reflux are presented in Fig. 1.(b) Molecular clearance from CSF and parenchyma of the entorhinal

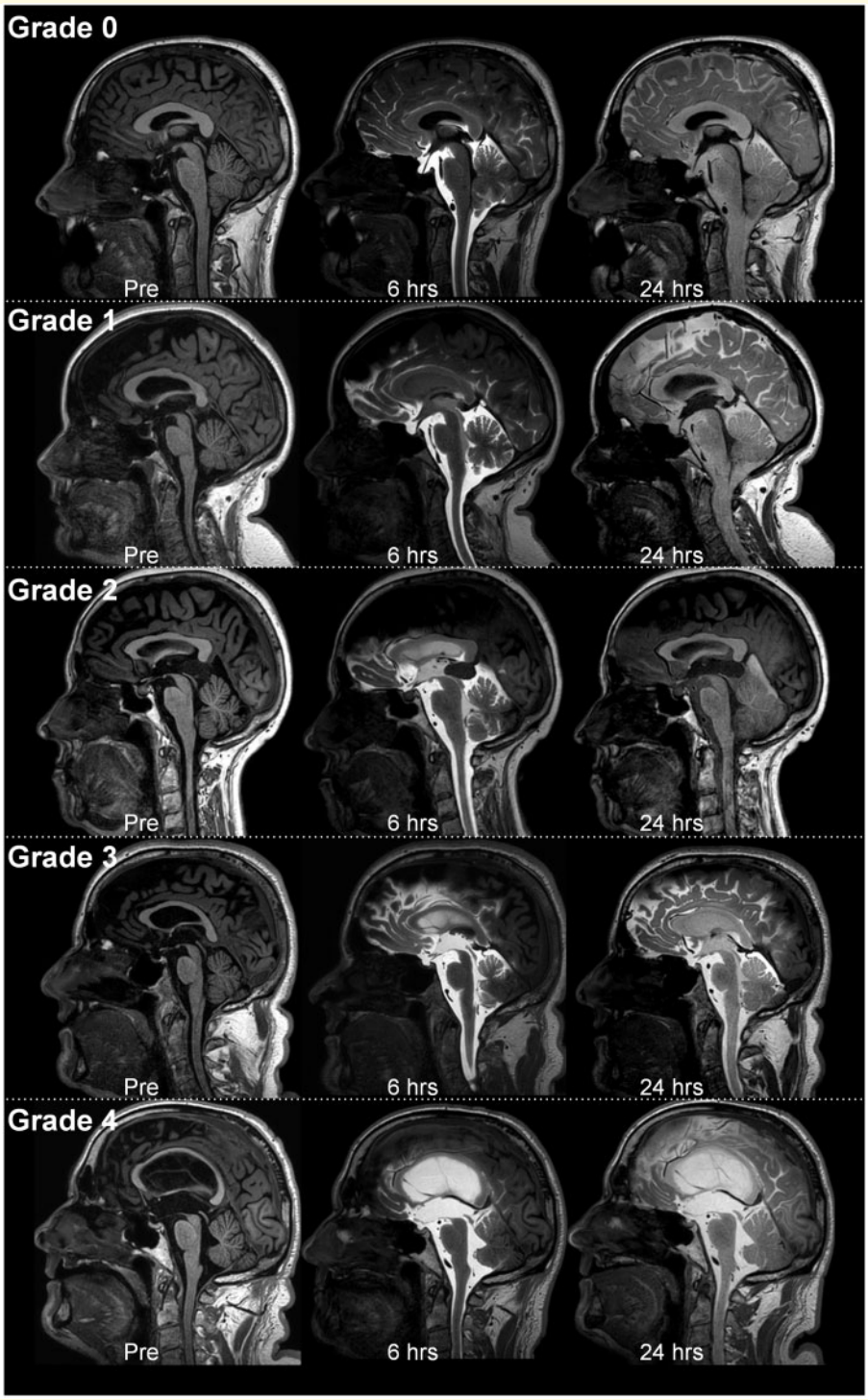

Figure 1 Grading of ventricular reflux. We categorized ventricular reflux in five categories: (**A**) Grade 0: No supra-aqueductal reflux. (**B**) Grade 1: Sign of supra-aqueductal reflux. (**C**) Grade 2: Transient enrichment of lateral ventricles Day 1. (**D**) Grade 3: Lasting enrichment of lateral ventricles Day 2 (not isointense with CSF subarachnoid). (**E**) Grade 4: Lasting enrichment of lateral ventricles Day 2 (isointense with CSF subarachnoid). This illustration shows the gMRI for one individual for each of the ventricular reflux grades. The ventricular reflux grades 3–4 are typical features of iNPH

cortex (ERC). For each time point, circular regions of interest (ROIs) were placed both in the CSF of cisterna magna on 1 mm thick, axially reconstructed T1-weighted images and inside ERC directly on 1 mm thick, coronally reconstructed T1-weighted images at the level of the hippocampal sulcus. Measurements were done directly in the

hospital Picture archiving and communication system (Sectra IDS7, Sectra, Sweden), where each ROI provides the mean T1 signal intensity (in signal units) from the image greyscale and was normalized against a reference ROI by dividing measured T1 intensity from CSF or ERC with the value of the reference ROI to correct for any baseline changes of image grey scale due to image scaling. The reference ROI was placed within the posterior part of the superior sagittal sinus in axially reconstructed images from the same T1 volume scan. We have previously not detected any sign of contrast enhancement in this location after intrathecal gadobutrol (0.5 mmol). The ROIs were manually fitted to local anatomy to avoid partial volume effects from neighbouring tissue or CSF. For the CSF in cisterna magna, a single ROI was placed. For all pairwise ERC locations, the normalized T1 intensities from bilateral ROIs were determined and the average calculated. From previous experience with the current gMRI protocol, tracer enhancement in CSF peaked on Day 1 and had declined on Day 2 (Ringstad *et al.*, 2018). We defined one-night clearance as the percentage change in normalized T1 signal ratio from last MRI Day 1 until first MRI Day 2, and two-night clearance was defined by the percentage change in normalized T1 signal ratio from last MRI Day 1 until first MRI Day 3.

Magnetic resonance imaging biomarkers of CSF space anatomy

Evans' index was determined from T1-weighted axially reconstructed images (1 mm thickness) and represents the largest diameter of the frontal horns divided with the largest inner diameter of the cranium in the same slice (Brix *et al.*, 2017). The callosal angle was measured on T1-weighted coronal images as the angle between lateral ventricles at the level of the posterior commissure, as previously described (Virhammar *et al.*, 2014). Disproportional enlarged subarachnoid space hydrocephalus (DESH) (Hashimoto *et al.*, 2010) was assessed on T1-weighted coronal images, scored as yes/no, and were characterized by the combination of (i) enlarged ventricles, (ii) widening of Sylvian fissure and (iii) tight upper convexities.

Magnetic resonance imaging biomarkers of neurodegeneration

We scored the patients with three sets of biomarkers indicative of neurodegeneration:

Medial temporal atrophy (MTA) was categorized using the Schelten's score (Scheltens *et al.*, 1992) that is based on a visual rating of the width of the choroid fissure, the width of the temporal horn, and the height of the hippocampal formation: Score 0 (no atrophy), Score 1 (only widening of choroid fissure), Score 2 (also widening of the temporal horn of lateral ventricle), Score 3 (moderate loss of hippocampal volume, decrease in height) and Score 4 (severe volume loss of hippocampus).

The Fazeka's scale for white matter lesions (Fazekas *et al.*, 2002) differentiates four scores: Score 0: None or a single punctate white matter hyperintensity lesion. Score 1: Multiple punctate lesions. Score 2: Beginning confluence of lesions (bridging). Score 3: Large confluent lesions.

ERC thickness was determined as previously described (Eide and Ringstad, 2019) on coronally reconstructed T1 volume acquisitions with 1 mm slice thickness at the level of the hippocampal sulcus and measured from the ERC surface to the grey/white matter interface, and mid-way between the tentative location of parasubiculum and perirhinal cortex.

Pulsatile ICP score indicative of intracranial compliance

In this neurosurgical department, overnight monitoring of pulsatile ICP has been part of the clinical routine of assessment of iNPH since early 2000, based on the concept that the MWA is indicative of intracranial compliance (pressure–volume reserve capacity). The procedure of measuring ICP was previously described in detail (Eide and Sorteberg, 2010). In local anaesthesia, a burr hole is made in the right frontal region, and an ICP sensor (usually Codman, Johnson & Johnson, Raynham, MA, USA, and in some cases Raumedic NeuroVent P sensor, Raumedic AG, Münchberg, GE) is introduced 1–2 cm into the brain parenchyma after being tunnelled subcutaneously. Digital high-frequency monitoring is continued overnight, incorporating identification of the cardiac induced single pressure waves. The pulsatile ICP is characterized by the MWA (MWA), determined over 6 s time windows as average of diastolic/systolic pressure differences of the identified single pressure waves during every 6-s time window. The overnight MWA is represented by the average for all 6-s time windows.

The neurosurgical department's criteria for shunt surgery are fulfilment of diagnostic criteria for probable or possible iNPH in addition to results of ICP monitoring that fulfil the previously established criteria for having above-threshold MWAs (Eide and Sorteberg, 2010). In previous studies, shunt response was reported in 9/10 individuals with MWA on average overnight $\geq$4 mmHg and $\geq$5 mmHg in at least 10% of measurement time (Eide and Sorteberg, 2010).

A subset of REF subjects also underwent ICP measurement with determination of MWA, similar to that performed in iNPH subjects and as part of the diagnostic assessment.

Statistical analyses

Continuous or categorical data are presented as mean with standard deviation or number of patients and

percentages, when appropriate. Group difference between categorical or continuous data was assessed with Pearson χ^2 test or independent samples *t*-test, respectively. Logistic regression assessed the predictors of iNPH with the estimated c-statistics from each model. The c-statistics (equivalent to the area under the receiver operating characteristics curve) is a measure of the predictive accuracy of a logistic regression model. We estimated the empirically diagnostic cut-point using the methods implemented in the user-developed command cutpt in Stata with corresponding estimates for sensitivity, specificity and area under the receiver operating characteristics curve. Statistical significance was accepted at the 0.05 level. The statistical analysis was performed using Stata 15.0 (StataCorp LP, College Station, TX).

Data availability

The data supporting the findings of this study are available from the corresponding author upon reasonable request.

Results

Patient cohorts

From the gMRI database, we retrieved 34 iNPH patients and 17 REF subjects who were treated within the Department of Neurosurgery, Oslo University Hospital-Rikshospitalet during the period from year September 2015 to December 2019. The present data and proposed MRI biomarkers have previously not been presented.

Information about the patient cohorts is shown in Table 1. The iNPH cases differed from the REF subjects in several ways, they were significantly older than iNPH patients, and the gender distribution was different.

Magnetic resonance imaging biomarkers of CSF tracer dynamics, CSF space anatomy and neurodegeneration

The time course of tracer enrichment within CSF of cisterna magna is shown in Fig. 2A and within the parenchyma of ERC in Fig. 2B; tracer enrichment is presented as percentage change of normalized T1 signal unit ratios from before intrathecal gadobutrol (CSF tracer). In iNPH patients, the enrichment of CSF tracer is slower, while CSF tracer levels remain higher 24 and 48 h after intrathecal administration.

Ventricular tracer reflux in any degree was found in all patients diagnosed with Definite iNPH. Grades 3–4 ventricular reflux were observed in 31/34 (91%) of Definite iNPH patients, as compared with 2/17 (12%) REF subjects (Table 2).

The one-night clearance (i.e. reduction of normalized signal unit ratio from last MRI Day 1 to first MRI Day 2) was significantly delayed in CSF as well as ERC of iNPH patients (Table 2). Two-night clearance (i.e. reduction of normalized signal unit ratio from last MRI

Table 1 Demographic and clinical information about the iNPH and REF cohorts

	iNPH	REF	Test statistic	*P*-value
N	34	17		
Sex (F/M)	10/24	13/4	$\chi^2(1) = 10.136$	=0.001
Age (years)	70.5 ± 6.8	48.8 ± 10.8	$t(49) = 11.749$	<0.001
BMI (kg/m^2)	27.2 ± 4.3	28.0 ± 4.8	$t(49) = 0.602$	0.53
Symptoms reported by patient and/or family				
Gait disturbance	34 (100%)	0	$\chi^2(1) = 51.000$	<0.001
Urinary incontinence	24 (71%)	0	$\chi^2(1) = 22.667$	<0.001
Cognitive impairment	31 (91%)	5 (29%)	$\chi^2(1) = 20.825$	<0.001
Headache	3 (9%)	15 (88%)	$\chi^2(1) = 31.296$	<0.001
Dizziness	8 (24%)	5 (29%)	$\chi^2(1) = 0.207$	0.650
Lethargy	4 (12%)	6 (35%)	$\chi^2(1) = 3.981$	=0.045
Duration of symptoms (years)	3.2 ± 2.7	3.7 ± 1.9	$t(49) = 0.682$	0.498
Pre-shunt NPH-score	12 (8–13)	15 (14–15)	$t(49) = 10.439$	<0.001
Tests of cognitive function				
Mini-mental state (MMS)	28 (14–30)			
Montreal Cognitive Assessment (MoCA)	21 (17–29)			
Overnight MWA				
N	33	5		
Number of 6-s time windows	5155 ± 2288	4584 ± 2582	$t(36) = 0.512$	0.612
MWA, average	5.9 ± 1.8	3.0 ± 0.7	$t(36) = 3.528$	=0.002
MWA, % >5 mmHg	55.4 ± 31.2	4.2 ± 5.0	$t(36) = 3.621$	=0.001
Surgical responders	34 (100%)			
Post-shunt NPH-score	14 (11–15)			

Categorical data presented as numbers; continuous data presented as mean ± standard deviation or (minimum – maximum), NPH-scores, MMS and MoCA presented as median (ranges in parentheses). Significant differences between groups were determined by Pearson χ^2 test for categorical data and by independent samples *t*-test for continuous data. iNPH = idiopathic normal pressure hydrocephalus; MWA = mean ICP wave amplitude; REF = reference patients.

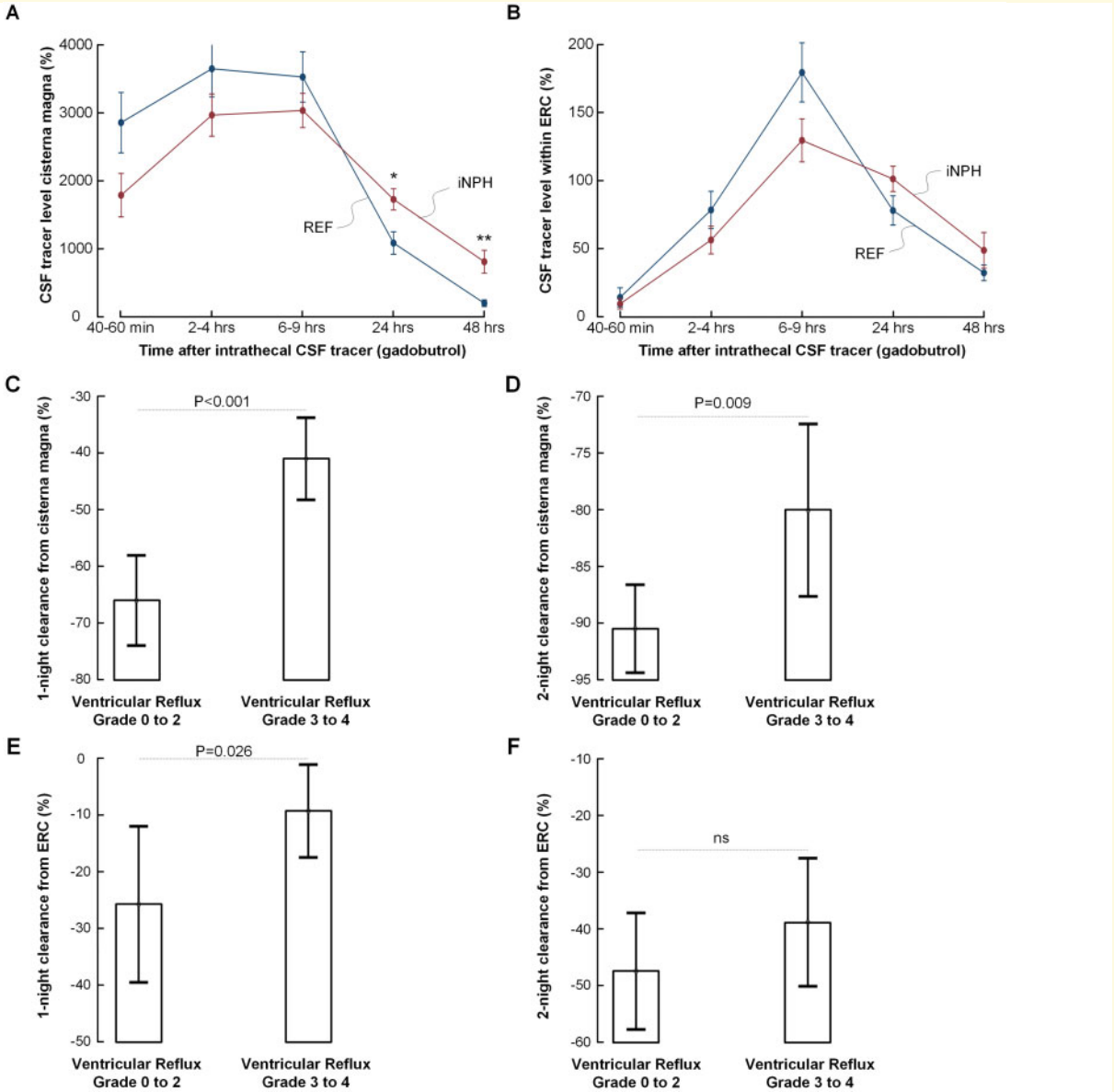

Figure 2 Molecular clearance from CSF and brain parenchyma and association with ventricular reflux. Comparison of time course of CSF tracer level within (**A**) CSF of cisterna magna and (**B**) parenchyma of ERC in iNPH ($n = 34$) and REF ($n = 17$) subjects. The CSF tracer level is expressed as mean (standard error) percentage change of normalized signal unit ratio (*$P = 0.013$, ** $P < 0.001$; independent samples *t*-test). Comparisons of (**C**) one-night clearance ($n = 50$) and (**D**) two-night clearance ($n = 27$) of CSF tracer from cisterna magna in individuals with ventricular reflux grades 0–2 ($n = 18$) and 3–4 ($n = 33$). Both one- and two-night clearances were impaired in the individuals with ventricular reflux grades 3–4. Comparisons of (**E**) one-night clearance ($n = 50$) and (**F**) two-night clearance ($n = 27$) of CSF tracer from parenchyma of ERC in individuals with ventricular reflux grades 0–2 ($n = 18$) and 3–4 ($n = 33$) showed significantly impaired one-night clearance in individuals with ventricular reflux grades 3–4. Statistical differences are indicated, and were determined by independent samples *t*-test. Error bars 95% CI

Day 1 to MRI Day 3) was delayed significantly in CSF but did not reach significance in ERC of iNPH patients. Logistic regression analysis adjusting for age showed that ventricular reflux, and clearance from CSF and ERC, differentiated the patient cohorts (Table 2).

Higher scores of ventricular reflux (grades 3–4) were accompanied by reduced clearance of CSF tracer from both CSF and ERC. Both one- and two-night clearance of CSF tracer from cisterna magna was impaired in individuals with ventricular reflux grades 3–4 (Fig. 2C and D). Similarly, clearance from ERC was impaired the first night in patients with ventricular reflux grades 3–4 (Fig. 2E); this was not significant for two-night clearance (Fig. 2F).

The MRI biomarkers of CSF space anatomy, Evans' index, callosal angle and DESH, differed significantly

Table 2 MRI biomarkers of CSF tracer dynamics, CSF space anatomy and neurodegeneration in iNPH and REF subjects

MRI biomarkers						Logistic regression analysis			
		iNPH ($n = 34$)	REF ($n = 17$)	Test statistic	*P*-value	Odds ratio	95% CI	*P*-value	C-statistics
CSF tracer dynamics									
Ventricular reflux	Grade 0	0 (0%)	6 (35%)						
	Grade 1	2 (6%)	4 (24%)						
	Grade 2	1 (3%)	5 (29%)	$\chi^2(4) = 33.887$	<0.001	3.2	1.1–8.9	=0.026	0.97
	Grade 3	9 (26%)	2 (12%)						
	Grade 4	22 (65%)	0 (0%)						
Clearance of CSF tracer	CSF (one-night clearance)	−41 ± 20	−69 ± 13	$t(49) = 5.232$	<0.001	1.09	1.01–1.18	0.028	0.97
	CSF (two-night clearance)	−78 ± 12	−92 ± 5	$t(49) = 4.597$	<0.001	1.40	0.98–2.0	0.066	0.98
	ERC (one-night clearance)	−7 ± 23	−31 ± 24	$t(49) = 3.463$	=0.001	1.08	1.0–1.16	0.047	0.96
	ERC (two-night clearance)	−37 ± 17	−49 ± 18	$t(49) = 2.331$	0.024	1.09	0.96–1.25	0.191	0.92
CSF space anatomy									
Evans index		0.39 ± 0.05	0.26 ± 0.03	$t(49) = 9.841$	<0.001				
Callosal angle		70.7 ± 24.1	114.9 ± 12.2	$t(49) = 7.096$	<0.001	0.94	0.90–0.99	=0.018	0.97
DESH	Present	15 (44%)	0		<0.001				
	Absent	19 (56%)	17 (100%)	$\chi^2(1) = 10.625$		3.31	0.33–∞	<0.001	NA
Biomarkers of neurodegeneration									
Scheltens MTA	Grade 0	0 (0%)	11 (65%)						
	Grade 1	2 (6%)	5 (29%)	$\chi^2(3) = 40.238$	<0.001	45.2	2.9–697.2	=0.006	0.98
	Grade 2	26 (76%)	1 (6%)						
	Grade 3	6 (18%)	0 (0%)						
Fazekas scale	Grade 0	3 (9%)	12 (70%)						
	Grade 1	11 (32%)	4 (24%)	$\chi^2(3) = 22.846$	<0.001	3.1	0.8–12.1	0.102	0.95
	Grade 2	12 (35%)	1 (6%)						
	Grade 3	8 (24%)	0 (0%)						
ERC thickness (mm)		1.90 ± 0.354	2.28 ± 0.27	$t(49) = 3.889$	<0.001	0.01	0–1.25	=0.062	0.96

Age-adjusted significance levels in logistic regression analysis were determined. one-night clearance: Percentage change in normalized signal unit ratio from last MRI Day 1 to MRI Day 2 (24 h). two-night clearance: percentage change in normalized signal unit ratio from last MRI Day 1 to MRI Day 3 (48 h). Significant differences between groups were determined by Pearson χ^2 test for categorical data and by independent samples *t*-test for continuous data.
The results of logistic regression analysis for Evans index are not presented because of extreme high values caused by nearly no overlap between groups. Odds ratio of DESH was estimated by exact logistic regression.

between iNPH and REF subjects, and logistic regression analysis adjusting for age showed that the anatomical biomarkers differentiated the patient cohorts (Table 2). Furthermore, the MRI biomarkers of neurodegeneration, Schelten's MTA score, Fazeka's score and ERC thickness, were all significantly different between iNPH patients and REF subjects (Table 2). Age-adjusted logistic regression analysis showed that Schelten's MTA score and ERC thickness significantly differentiated the patient cohorts (Table 2).

We further found a highly significant correlation between the MRI biomarkers of CSF tracer dynamics and biomarkers of CSF space anatomy and neurodegeneration (Table 3). Increasing ventricular reflux grade was positively correlated with Evans index, Schelten's MTA score and Fazeka's score, and negatively correlated with callosal angle and ERC thickness. Similarly, reduced CSF tracer clearance was positively correlated with increased Evans index, Schelten's MTA score and Fazeka's score, while negatively correlated with reduced callosal angle and reduced ERC thickness (Table 3). Moreover, as compared with individuals without signs of DESH, subjects with presence of DESH presented with higher ventricular reflux scores ($n = 51$; Pearson χ^2 test $\chi^2(4) = 9.329$, $P = 0.05$), and reduced one-night clearance of CSF tracer from CSF ($n = 50$; independent samples *t*-test $t(48) = 2.021$, $P = 0.049$).

Table 4 provides an overview of the predictive ability of cut-point values for the different MRI biomarkers with regard to the ability of differentiating iNPH patients from REF subjects. Based on the estimated area under the receiver operating characteristics curve, the biomarkers Evans index, ventricular reflux, one-night clearance from CSF and Schelten's MTA had the highest diagnostic ability, all with area under the receiver operating characteristics curve ≥0.85. These four biomarkers had reasonable high sensitivity and specificity.

The MRI biomarkers at individual level are presented in Supplementary Table 1.

Table 3 Correlations between biomarkers of CSF tracer dynamics and biomarkers of CSF space anatomy and neurodegeneration

MRI biomarkers of CSF tracer dynamics	MRI biomarkers of CSF space anatomy		MRI biomarkers of neurodegeneration		
	Evans' index ($n = 51$)	Callosal angle ($n = 51$)	Schelten's MTA ($n = 50$)	Fazeka's scale ($n = 51$)	ERC thickness ($n = 50$)
Ventricular reflux					
Ventricular reflux grade ($n = 51$)	$r = 0.76$ ($P < 0.001$)	$r = -0.70$ ($P < 0.001$)	$r_s = 0.78$ ($P < 0.001$)	$r_s = 0.54$ ($P < 0.001$)	$r = -0.46$ ($P = 0.001$)
Clearance of CSF tracer					
CSF (one-night clearance; $n = 50$)	$r = 0.53$ ($P < 0.001$)	$r = -0.45$ ($P = 0.001$)	$r_s = 0.46$ ($P = 0.001$)	$r_s = 0.29$ ($P = 0.041$)	$r = -0.33$ ($P = 0.018$)
CSF (two-night clearance; $n = 27$)	$r = 0.57$ ($P = 0.002$)	$r = -0.37$ (0.052)	$r_s = 0.60$ ($P = 0.001$)	$r_s = 0.37$ (0.057)	$r = -0.47$ ($P = 0.014$)
ERC (one-night clearance; $n = 50$)	$r = 0.42$ ($P = 0.003$)	$r = -0.28$ (0.052)	$r_s = 0.35$ ($P = 0.013$)	$r_s = 0.31$ (0.026)	$r = -0.14$ (0.303)
ERC (two-night clearance; $n = 27$)	$r = 0.46$ ($P = 0.016$)	$r = -0.67$ ($P < 0.001$)	$r_s = 0.37$ (0.061)	$r_s = 0.25$ (0.207)	$r = -0.34$ ($P = 0.015$)

r_s = Spearman correlation coefficients determined for categorical data. r = Pearson correlation coefficients determined for continuous data.

Table 4 Optimal cut-points for the different MRI biomarkers

MRI biomarkers	Differentiation between iNPH and REF			
	Cut-point	Sensitivity	Specificity	Area ROC
CSF tracer dynamics	>			
Ventricular reflux (0/1/2/3/4)	2	0.91	0.88	0.90
CSF one-night clearance (%)	−53	0.82	0.88	0.85
CSF two-night clearance (%)	−92	0.91	0.69	0.80
ERC one-night clearance (%)	−25	0.76	0.71	0.73
ERC two-night clearance (%)	−50	0.82	0.56	0.69
CSF space anatomy	>			
Evans index	0.31	0.97	0.94	0.96
Callosal angle (degrees)	126	0.06	0.82	0.44
DESH (Yes/No)[a]	0	0.44	1.00	0.72
Neurodegeneration	>			
Schelten's MTA (0/1/2/3)	1	0.94	0.94	0.94
Fazeka's scale (0/1/2/3)	0	0.91	0.71	0.81
ERC thickness (mm)	2	0.42	0.24	0.33

ROC = receiver operating characteristics.
[a]No reference subjects in our cohort presented with DESH signs.

Magnetic resonance imaging biomarkers versus ICP biomarkers of impaired intracranial compliance

The pulsatile ICP (MWA) measured overnight was significantly higher in iNPH subjects ($n = 33$) than in REF subjects ($n = 5$; Table 1). In all iNPH patients, the MWA scores were above the previously established criteria (Eide and Sorteberg, 2010) but were below established criteria in all REF subjects.

The relationship between average MWA score overnight and the different MRI biomarkers are shown in Fig. 3. The ventricular reflux grades 3–4 were accompanied by significantly increased MWA scores (Fig. 3A). Grades 3–4 ventricular reflux were seen in 0/5 (0%) individuals with MWA scores below thresholds while in 30/33 (91%) individuals with MWA above thresholds. Moreover, as compared to individuals with MWA scores below thresholds, patients with MWA levels above defined thresholds had significantly reduced clearance capacity from CSF (Fig. 3B) and from the ERC (Fig. 3C).

The MWA-scores indicative of intracranial compliance related to CSF space anatomy, as overnight average MWA increased with increasing Evans (Fig. 3D). With increasing MWA, the callosal angle became narrower (Fig. 3E), and in those with DESH signs, the MWA was increased (Fig. 3F).

Also, the MRI scores indicative of neurodegeneration were associated with the MWA scores. The average MWA overnight was significantly increased in individuals with Schelten's MTA score 2–3 (Fig. 3G) and in individuals with Fazeka's score 2–3 (Fig. 3H). Moreover, there was a significant negative correlation between ERC thickness and MWA levels.

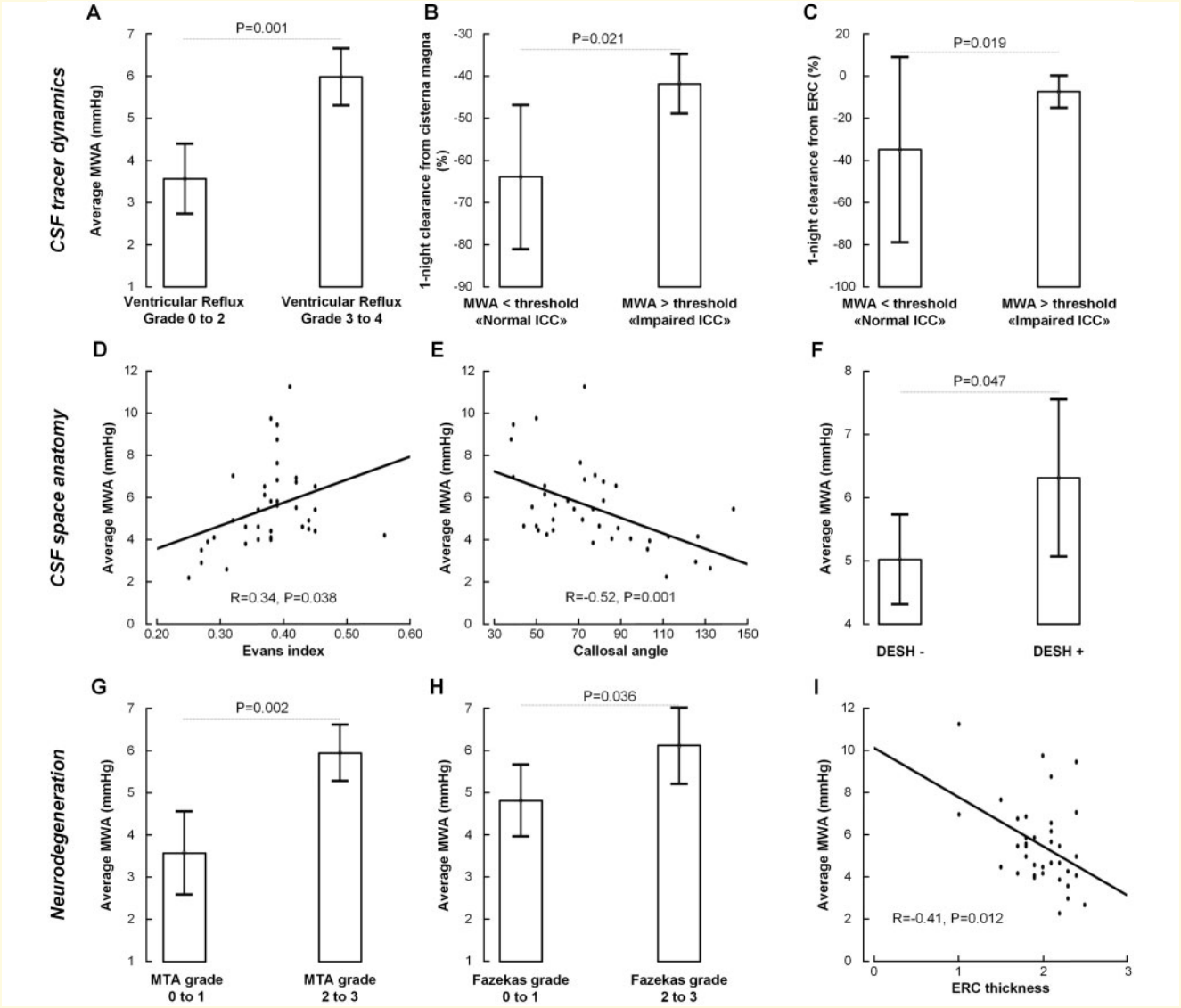

Figure 3 Association between pulsatile ICP and MRI biomarkers of CSF tracer dynamics, CSF space anatomy, and neurodegeneration. The MWA, which is indicative of the intracranial compliance, associate significantly with the MRI biomarkers of CSF tracer dynamics (**A–C**), CSF space anatomy (**D–F**) and neurodegeneration (**G–I**). *CSF tracer dynamics:* (**A**) Comparison of overnight average MWA scores in individuals with ventricular reflux grades 0–2 ($n = 18$) and 3–4 ($n = 33$) shows significantly increased average levels of MWA in the individuals with ventricular reflux grades 3–4. The MWA level in this latter group was above established thresholds (Eide and Sorteberg, 2010). Moreover, individuals with overnight MWA above established thresholds ($n = 33$), indicative of impaired intracranial compliance, presented with significantly (**B**) reduced one-night clearance from CSF, and (**C**) reduced one-night clearance of CSF tracer from ERC. *CSF space anatomy:* There was (**A**) a significant positive correlation between overnight average MWA and Evans' index ($n = 38$), (**B**) a significant negative correlation between callosal angle and average MWA ($m = 38$), and (**C**) the overnight MWA was significantly higher in individuals with positive DESH signs ($n = 38$). *Neurodegeneration:* The overnight MWA was (**D**) significantly higher in individuals with MTA grades 2–3 ($n = 33$) as compared with 0–1 ($n = 17$), (**E**) significantly higher in individuals with Fazeka's grades 2–3 ($n = 21$) versus 0–1 ($n = 30$). (**F**) Moreover, there is significant correlation between overnight average MWA and ERC thickness ($n = 37$). Significance levels were determined by independent samples *t*-test. For scatter plots are shown the fit lines and Pearson correlation coefficients with significance levels. Error bars 95% CI

Discussion

In this study, we report *in vivo* evidence of impaired molecular clearance from CSF and parenchyma of ERC in shunt-responsive iNPH ('Definite iNPH') and identify new MRI biomarkers of CSF tracer dynamics that may add favourably to anatomically derived MRI biomarkers. The reasoned anticipation that the applied tracer molecule (gadobutrol) is cleared along the same extra-vascular pathways as tau protein and some neurotoxic

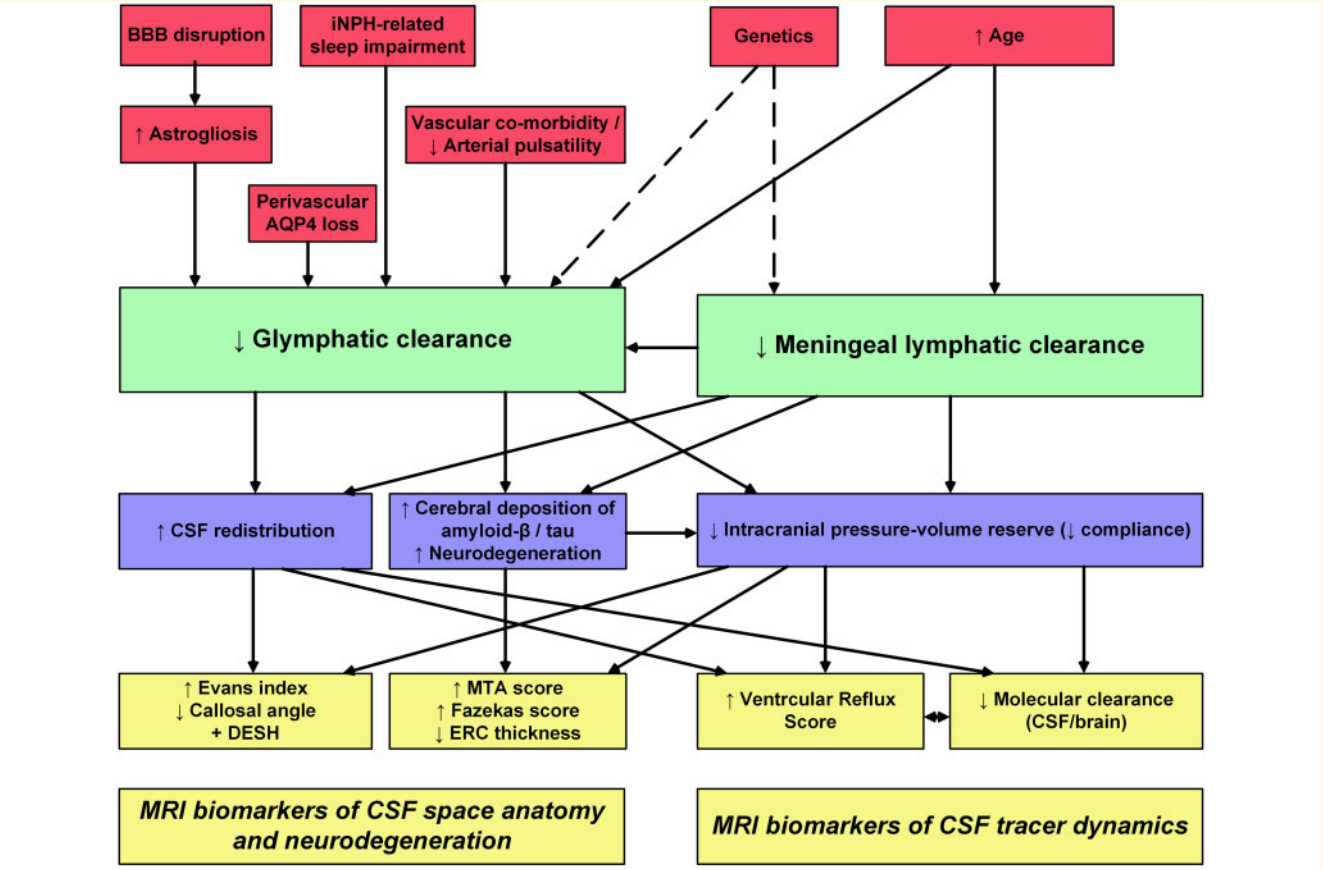

Figure 4 Rationale for utility of established and proposed MRI biomarkers for iNPH disease. The diagram provides an overview of our rational for the previously established and presently proposed MRI biomarkers of iNPH disease. Possible etiological factors in iNPH are indicated (red boxes). We propose that failure of glymphatic and meningeal lymphatic function may be key features of iNPH (green boxes). The possible consequences of impaired glymphatic and meningeal lymphatic function are indicated (blue boxes), as well as the MRI biomarkers that may be suggestive of iNPH pathogenesis (yellow boxes)

amyloid-β isoforms may bridge previous findings of overlapping amyloid-β and tau pathology in brain tissue of iNPH and Alzheimer's disease.

In Fig. 4, we have summarized possible mechanisms behind the novel MRI biomarkers for visualization of CSF tracer dynamics (i.e. CSF ventricular reflux grade and molecular clearance from brain and CSF spaces) in addition to the traditional MRI biomarkers of CSF space anatomy (Evans index, callosal angle and the presence of DESH sign) and neurodegeneration (MTA score, Fazekas score and ERC thickness). While the anatomical MRI biomarkers have been used for years, the biomarkers of CSF tracer dynamics (ventricular reflux grade and molecular clearance) are novel.

The aetiology of iNPH remains unknown, but some mechanisms have been proposed. Cortical brain biopsies from iNPH patients show marked alterations at the glia-vascular interface (i.e. neurovascular unit), including loss of the water channel aquaporin-4 at astrocytic perivascular endfeet (Eide and Hansson, 2018; Hasan-Olive *et al.*, 2019), and basement membrane alterations including pericyte degeneration (Eidsvaag *et al.*, 2017), furthermore a defective BBB with leakage of blood products such as fibrinogen (Eide and Hansson, 2020), which is pro-inflammatory and a possible cause of astrogliosis that characterizes the iNPH brain (Eide and Hansson, 2018). In iNPH, mitochondrial pathology is present in perivascular astrocytic endfeet and in neurons with evidence of altered cellular clearance (Hasan-Olive *et al.*, 2019). Astrogliosis would be expected to affect the physical dimensions of the perivascular spaces and aquaporin-4 loss might impair the fluid turnover in perivascular spaces (Nagelhus and Ottersen, 2013). Most likely, genetic factors are at play in iNPH pathogenesis (Korhonen *et al.*, 2018).

The degree of ventricular reflux of CSF tracer in Definite iNPH was high. Reflux of tracer into the supra-aqueductal brain ventricles was previously assessed using radioactive tracer and nuclear imaging in the selection of iNPH patients to shunting (Vanneste *et al.*, 1992; Algin *et al.*, 2011), but was more or less abandoned (Vanneste *et al.*, 1992). The mechanism behind such reflux in NPH has never been well understood. A potential factor might

be mixing with CSF in the state of hyperdynamic, bidirectional CSF flow pulsatility (i.e. dispersion) at level with the aqueduct or even net retrograde CSF flow into the ventricular compartment. This has later been examined using phase-contrast MRI (Lindstrom *et al.*, 2018), though this modality has methodological weaknesses. Here, we introduce a clinically feasible grading of ventricular CSF tracer enrichment based on visual inspection of T1 images. Reflux grades 3–4 were associated with MWA above threshold values from ICP (Fig. 3A), which has previously shown high predictive value for a beneficial shunt response (Eide and Sorteberg, 2010). High reflux grade also correlated positively with Evans' index and DESH, and negatively with callosal angle, suggesting ventricular CSF reflux has a pathogenic role in ventricular enlargement and the upward movement of the brain along the z-axis in iNPH (Yamada *et al.*, 2015). It may be postulated that resistance to the CSF movement causes the CSF tracer to redistribute to the ventricular compartment, most likely as an alternative clearance route along the path of least resistance. It has for long been assumed that resistance to CSF outflow due to obstruction at the arachnoid granulations is a key mechanism behind iNPH, and the rationale behind the lumbar and ventricular infusion tests (Marmarou *et al.*, 2005; Qvarlander *et al.*, 2014). While the infusion tests have focused on water exchange in a hydraulic model, the present data highlight the metabolic aspect of iNPH disease.

Recent, groundbreaking findings of glymphatic and meningeal lymphatic molecular clearance failure in neurodegenerative disease (Da Mesquita *et al.*, 2018; Sweeney and Zlokovic, 2018; Zou *et al.*, 2019; Reeves *et al.*, 2020) still await translation into the clinic and patient treatment. It is reasonable that the combined impairment of glymphatic and meningeal lymphatic functions are major players behind iNPH disease. In the CSF spaces surrounding vessels that are visible at the brain surface by gMRI, the pace of tracer propagation is significantly slower in iNPH than REF subjects (Ringstad *et al.*, 2017). Other factors that might affect perivascular (glymphatic) transport are vascular co-morbidity impairing arterial pulsations such as arterial hypertension and diabetes, both being prevalent in iNPH (Eide and Pripp, 2014). Arterial hypertension reduces peri-arterial molecular movement by reducing arterial wall pulsations (Mestre *et al.*, 2018), and diabetes seems to impair the glymphatic function (Jiang *et al.*, 2017). The prevalence of iNPH increases substantially with increasing age (Brean and Eide, 2008). Increasing age was also shown to impair glymphatic function in rodents (Kress *et al.*, 2014). Furthermore, experimental evidence from rodents suggests that meningeal lymphatic function becomes reduced with increasing age (Ma *et al.*, 2017). Given that the glymphatic system is most active during sleep (Xie *et al.*, 2013), it is notable that sleep disturbance is prevalent in iNPH (Roman *et al.*, 2019). In our gMRI studies, we have provided evidence of markedly reduced extravascular transport of a CSF tracer in iNPH (Ringstad *et al.*, 2017; Ringstad *et al.*, 2018; Eide *et al.*, 2019), indicative of impaired glymphatic function. A recent modelling study of the tracer movement supports the hypothesis of convective forces behind molecular transport within the human brain (Valnes *et al.*, 2020). One important observation from gMRI is that enrichment of tracer in the brain is highly associated with enrichment in CSF spaces at the adjacent brain surface (Ringstad *et al.*, 2017; Eide and Ringstad, 2019). Delayed clearance of tracer from subarachnoid CSF spaces would be expected to result in delayed glymphatic clearance of the tracer. Thus, impaired meningeal lymphatic clearance may be a major determinant for impaired glymphatic function in iNPH. We recently provided evidence of direct molecular efflux from subarachnoid CSF to parasagittal dura (Ringstad and Eide, 2020), which may be a bridging link between brain/CSF and the meningeal lymphatic system.

Gadobutrol administered intrathecally distributes in the CSF and the extra-vascular spaces of the brain as it in principle does not cross the healthy BBB (Cheng, 2004). Similarly, potential neurotoxic proteins from brain metabolism such as tau and some soluble amyloid-β isomers are cleared along extravascular pathways (Jawhar *et al.*, 2011; Iliff *et al.*, 2014). Tau has no known BBB transporter. Some amyloid-β isoforms have BBB transporter while the most toxic isoforms seem to clear via the extravascular compartment (Rissman *et al.*, 2012; Chai *et al.*, 2020). Gadobutrol is a useful CSF tracer as it is a highly hydrophilic compound, with an estimated hydraulic diameter of less than 2 nm (Ringstad *et al.*, 2018). It is expected to pass between the perivascular and interstitial space through astrocytic endfeet gaps, which are about 20 nm. The outer diameter of amyloid-β oligomers is as well <20 nm (Sakono and Zako, 2010). Therefore, even though the gadobutrol molecule is small, clearance of this molecule may reflect the clearance of endogenous metabolites such as amyloid-β and tau.

It is increasingly acknowledged that iNPH is a neurodegenerative disease (Hasan-Olive *et al.*, 2019), and the possible role of failure of glymphatic function in iNPH was recently reviewed (Reeves *et al.*, 2020). In animal studies, impaired aquaporin-4 dependent glymphatic function caused delayed clearance of metabolites such as amyloid-β (Iliff *et al.*, 2012). Thus, it may be speculated that impaired paravascular (or glymphatic) function in iNPH is contributing to amyloid-β deposition in these individuals. It is well established that iNPH show deposition of amyloid-β and tau in a substantial proportion of patients suggesting an overlap with Alzheimer's disease in one-third to half of the iNPH patients (Leinonen *et al.*, 2010). Characteristics of iNPH such as neurodegeneration and toxic metabolite deposition indicate that iNPH may even serve as a model disease of Alzheimer's disease

(Libard and Alafuzoff, 2019). Accordingly, delayed clearance of toxic metabolites may be a crucial player behind the neurodegeneration characterizing iNPH.

Traditional radiological biomarkers of CSF space anatomy in iNPH include Evans index (Brix *et al.*, 2017), callosal angle (Virhammar *et al.*, 2014), DESH (Hashimoto *et al.*, 2010) and combinations thereof (Kockum *et al.*, 2018) that differentiate iNPH from non-iNPH subjects. The ventricular reflux could be causative for ventricular enlargement, and cranial displacement of ventricles with reduced callosal angle and convexity block. We suggest the combined impairment of glymphatic and meningeal lymphatic function might be expected to result in increased resistance to CSF flow and redistribution of CSF, including redirection of CSF flow to ventricles (i.e. ventricular reflux). Notably, the presence of iNPH disease may not necessarily imply a shunt response. The American-European criteria of iNPH (Relkin *et al.*, 2005) state that even a patient fulfils the criteria of Probable iNPH, it does not necessarily mean that the individual is shunt-responsive. The guidelines also differentiate between shunt-responsive and shunt non-responsive iNPH (Relkin *et al.*, 2005). However, since shunt is the only effective treatment for iNPH, several additional tests have been developed to predict shunt response, such as infusion tests, temporary lumbar CSF drainage and ICP monitoring (Marmarou *et al.*, 2005).

Since early 2000, we have performed overnight ICP monitoring with determination of the MWA. The proportion of clinical iNPH shunt responders among patients with MWA above-defined thresholds (Eide and Sorteberg, 2010) is comparable with another approach, namely extended lumbar drainage that predict shunt response with comparable accuracy (Marmarou *et al.*, 2005). The rationale is that increased MWA provides an indirect measure of impaired intracranial compliance (i.e. reduced pressure-volume reserve capacity) (Eide and Sorteberg, 2007; Eide, 2016). Intracranial compliance is typically impaired in states of compromised run-off of venous blood (as in venous sinus thrombosis) or CSF (as in obstructive hydrocephalus), or impaired CSF runoff secondary to both impaired glymphatic and meningeal lymphatic function. Increased MWA, indicative of impaired intracranial compliance, was accompanied by abnormal CSF tracer dynamics (illustrated by an increased degree of ventricular reflux and reduced clearance from CSF and ERC) and was associated with altered CSF space anatomy and an increasing degree of neurodegeneration. Further studies are needed to decipher whether altered compliance is a factor in neurodegeneration or whether neurodegeneration may be instrumental behind impaired compliance, the latter possibly due to a less elastic brain (Fattahi *et al.*, 2016).

The present study has some limitations that should be noted. First, the iNPH and REF subjects differed in several respects, as iNPH patients were older and with a different gender distribution. The reason is that gMRI is invasive and performed as a research study of various CSF circulation disorders, where one of them was iNPH. A clinical indication for gMRI was therefore present in all patients. Even though we included those subjects from the entire REF cohort closest in age with iNPH, the age differed significantly. As it has previously been reported that molecular clearance is reduced with ageing (Zhou *et al.*, 2020), differences between iNPH and REF subjects may to some extent be age-related. On the other hand, this study primarily focused on the comparison of MRI biomarkers and to which degree they differentiated iNPH from REF subjects, incorporating age-adjusted logistic regression analysis. We also compared the MRI biomarkers with other measures including pulsatile ICP (overnight MWA), which is less affected by age. However, we cannot exclude that the increased age in iNPH subjects explains some of the differences between iNPH and REF cohorts. Future studies comparing age-matched individuals with iNPH are needed to clarify the impact of age.

A potential limitation is that we included the only iNPH with shunt–response, i.e., definite iNPH. In the gMRI database, there were no shunt-non-responders. We could therefore not compare iNPH shunt responders versus non-responders. This is related to the very high degree of shunt response with the selection tool we use. On the other hand, the present study enabled comparison of individuals with overnight MWA below or above established thresholds that previously have been shown to efficiently differentiate iNPH shunt responders from non-responders (Eide and Sorteberg, 2010; Eide and Sorteberg, 2016).

Another obvious limitation is that the CSF tracer gadobutrol, a gadolinium-containing MRI contrast agent, is yet not approved for intrathecal use, but is, however, used quite commonly at many centers for imaging work-up of CSF leaks. In general, the use of MRI contrast agents is used with caution due to reports of gadolinium chelates found outside the BBB after intravenous use (Kanda *et al.*, 2014). In patient treatment, any risk should be weighed against the potential benefit. With high morbidity and 5-year mortality in iNPH (Jaraj *et al.*, 2017), efforts in the improved selection are justified, including ruling out those who would not benefit from surgery, as the complication rate with shunting is not negligible (Eide and Sorteberg, 2016). The safety profile of intrathecal gadobutrol is good and comparable to the on-label intrathecal administration of CT contrast agents (Edeklev *et al.*, 2019; Halvorsen *et al.*, 2020). Reports of retention in the brain after intravenous administration of macrocyclic contrast agents are rare (Radbruch *et al.*, 2017), and no evidence of retention after intrathecal administration has been detected (Ringstad *et al.*, 2018). Furthermore, intravenous doses (of typically 7.5–20 ml) are also shown to readily leak into CSF and circulate between the CSF and blood circulation for weeks thereafter (Nehra *et al.*, 2018).

Conclusions

Use of intrathecal CSF tracer demonstrated ventricular redistribution and impaired clearance of the tracer in shunt-responsive (Definite) iNPH. We suggest this primarily is caused by delayed glymphatic and meningeal lymphatic clearance function, and impaired intracranial compliance. The results may point to CSF molecular clearance failure in other dementias, particularly Alzheimer's disease, which have a high overlap with iNPH in tissue specimens. Minimally invasive diagnostics of impaired CSF clearance, which would be of particular interest in the early stages of neurodegenerative disease, may potentially also be utilized in other dementia-related proteinopathies. Here, biomarkers from gMRI added unique information of CSF dynamics and clearance to previously established anatomical MRI biomarkers in discriminating iNPH from reference patients and may potentially be a more disease-specific and less invasive alternative to other ancillary tests to identify shunt-responsive iNPH. Further studies are required to examine this.

Supplementary material

Supplementary material is available at *Brain Communications* online.

Acknowledgements

We thank Dr. Øivind Gjertsen, Dr. Bård Nedregaard and Dr. Ruth Sletteberg from the Department of Radiology, Oslo University Hospital – Rikshospitalet, who performed the intrathecal gadobutrol injections in all study subjects. We also sincerely thank the Intervention Centre and Department of Neurosurgery at Oslo University Hospital Rikshospitalet for providing valuable support with MR scanning and care-taking of all study subjects throughout the study. Finally, we sincerely thank the Nurse Staff and Hydrocephalus outward clinic, Department of Neurosurgery Oslo University Hospital – Rikshospitalet for care-taking of all study subjects throughout the study.

Funding

Department of Neurosurgery, Oslo University Hospital – Rikshospitalet.

Competing interests

The authors report no competing interests. G.R. has received a speaker fee from Bayer AG.

References

Algin O, Hakyemez B, Ocakoglu G, Parlak M. MR cisternography: is it useful in the diagnosis of normal-pressure hydrocephalus and the selection of "good shunt responders"? Diag Interv Radiol (Ankara, Turkey) 2011; 17: 105–11.

Brean A, Eide PK. Prevalence of probable idiopathic normal pressure hydrocephalus in a Norwegian population. Acta Neurol Scand 2008; 118: 48–53.

Brix MK, Westman E, Simmons A, Ringstad GA, Eide PK, Wagner-Larsen K, et al. The Evans' Index revisited: new cut-off levels for use in radiological assessment of ventricular enlargement in the elderly. Eur J Radiol 2017; 95: 28–32.

Cabral D, Beach TG, Vedders L, Sue LI, Jacobson S, Myers K, et al. Frequency of Alzheimer's disease pathology at autopsy in patients with clinical normal pressure hydrocephalus. Alzheimer's Dement 2011; 7: 509–13.

Chai AB, Leung GKF, Callaghan R, Gelissen IC. P-glycoprotein: a role in the export of amyloid-beta in Alzheimer's disease? FEBS J 2020; 287: 612–25.

Cheng KT. Gadobutrol. Molecular imaging and contrast agent database (MICAD). Bethesda (MD): National Center for Biotechnology Information (US); 2004.

Da Mesquita S, Louveau A, Vaccari A, Smirnov I, Cornelison RC, Kingsmore KM, et al. Functional aspects of meningeal lymphatics in ageing and Alzheimer's disease. Nature 2018; 560: 185–91.

Edeklev CS, Halvorsen M, Lovland G, Vatnehol SAS, Gjertsen O, Nedregaard B, et al. Intrathecal use of gadobutrol for glymphatic MR imaging: prospective safety study of 100 patients. Am J Neuroradiol 2019; 40: 1257–64.

Eide PK. The correlation between pulsatile intracranial pressure and indices of intracranial pressure-volume reserve capacity: results from ventricular infusion testing. J Neurosurg 2016; 125: 1493–503.

Eide PK, Hansson HA. Astrogliosis and impaired aquaporin-4 and dystrophin systems in idiopathic normal pressure hydrocephalus. Neuropathol Appl Neurobiol 2018; 44: 474–90.

Eide PK, Hansson HA. Blood-brain barrier leakage of blood proteins in idiopathic normal pressure hydrocephalus. Brain Res 2020; 1727: 146547.

Eide PK, Pripp AH. Increased prevalence of cardiovascular disease in idiopathic normal pressure hydrocephalus patients compared to a population-based cohort from the HUNT3 survey. Fluids Barriers CNS 2014; 11: 19.

Eide PK, Ringstad G. Delayed clearance of cerebrospinal fluid tracer from entorhinal cortex in idiopathic normal pressure hydrocephalus: a glymphatic magnetic resonance imaging study. J Cereb Blood Flow Metab 2019; 39: 1355–68.

Eide PK, Sorteberg W. Association among intracranial compliance, intracranial pulse pressure amplitude and intracranial pressure in patients with intracranial bleeds. Neurol Res 2007; 29: 798–802.

Eide PK, Sorteberg W. Diagnostic intracranial pressure monitoring and surgical management in idiopathic normal pressure hydrocephalus: a 6-year review of 214 patients. Neurosurgery 2010; 66: 80–91.

Eide PK, Sorteberg W. Outcome of surgery for idiopathic normal pressure hydrocephalus: Role of preoperative static and pulsatile intracranial pressure. World Neurosurg 2016; 86: 186–93 e1.

Eide PK, Valnes LM, Pripp AH, Mardal KA, Ringstad G. Delayed clearance of cerebrospinal fluid tracer from choroid plexus in idiopathic normal pressure hydrocephalus. J Cereb Blood Flow Metab 2019; 39: 1355–68.

Eide PK, Vatnehol SAS, Emblem KE, Ringstad G. Magnetic resonance imaging provides evidence of glymphatic drainage from human brain to cervical lymph nodes. Sci Rep 2018; 8: 7194.

Eidsvaag VA, Hansson HA, Heuser K, Nagelhus EA, Eide PK. Brain capillary ultrastructure in idiopathic normal pressure hydrocephalus:

relationship with static and pulsatile intracranial pressure. J Neuropathol Exp Neurol 2017; 76: 1034–45.
Fattahi N, Arani A, Perry A, Meyer F, Manduca A, Glaser K, et al. MR elastography demonstrates increased brain stiffness in normal pressure hydrocephalus. Am J Neuroradiol 2016; 37: 462–7.
Fazekas F, Barkhof F, Wahlund LO, Pantoni L, Erkinjuntti T, Scheltens P, et al. CT and MRI rating of white matter lesions. Cerebrovasc Dis 2002; 13: 31–6.
Halvorsen M, Edeklev CS, Fraser-Green J, Lovland G, Vatnehol SAS, Gjertsen O, et al. Off-label intrathecal use of gadobutrol: safety study and comparison of administration protocols. Neuroradiology 2020.
Hasan-Olive MM, Enger R, Hansson HA, Nagelhus EA, Eide PK. Loss of perivascular aquaporin-4 in idiopathic normal pressure hydrocephalus. Glia 2019; 67: 91–100.
Hasan-Olive MM, Enger R, Hansson HA, Nagelhus EA, Eide PK. Pathological mitochondria in neurons and perivascular astrocytic endfeet of idiopathic normal pressure hydrocephalus patients. Fluids Barriers CNS 2019; 16: 39.
Hashimoto M, Ishikawa M, Mori E, Kuwana N; The study of INPH on neurological improvement (SINPHONI). Diagnosis of idiopathic normal pressure hydrocephalus is supported by MRI-based scheme: a prospective cohort study. Fluids Barriers CNS 2010; 7: 18.
Iliff JJ, Chen MJ, Plog BA, Zeppenfeld DM, Soltero M, Yang L, et al. Impairment of glymphatic pathway function promotes tau pathology after traumatic brain injury. J Neurosci 2014; 34: 16180–93.
Iliff JJ, Wang M, Liao Y, Plogg BA, Peng W, Gundersen GA, et al. A paravascular pathway facilitates CSF flow through the brain parenchyma and the clearance of interstitial solutes, including amyloid beta. Sci Transl Med 2012; 4: 147ra111.
Jaraj D, Wikkelso C, Rabiei K, Marlow T, Jensen C, Ostling S, et al. Mortality and risk of dementia in normal-pressure hydrocephalus: a population study. Alzheimer's Dement 2017; 13: 850–7.
Jawhar S, Wirths O, Bayer TA. Pyroglutamate amyloid-beta (Abeta): a hatchet man in Alzheimer disease. J Biol Chem 2011; 286: 38825–32.
Jiang Q, Zhang L, Ding G, Davoodi-Bojd E, Li Q, Li L, et al. Impairment of the glymphatic system after diabetes. J Cereb Blood Flow Metab 2017; 37: 1326–37.
Kanda T, Ishii K, Kawaguchi H, Kitajima K, Takenaka D. High signal intensity in the dentate nucleus and globus pallidus on unenhanced T1-weighted MR images: relationship with increasing cumulative dose of a gadolinium-based contrast material. Radiology 2014; 270: 834–41.
Kockum K, Lilja-Lund O, Larsson EM, Rosell M, Soderstrom L, Virhammar J, et al. The idiopathic normal-pressure hydrocephalus Radscale: a radiological scale for structured evaluation. Eur J Neurol 2018; 25: 569–76.
Korhonen VE, Helisalmi S, Jokinen A, Jokinen I, Lehtola JM, Oinas M, et al. Copy number loss in SFMBT1 is common among Finnish and Norwegian patients with iNPH. Neurol Genet 2018; 4: e291.
Kress BT, Iliff JJ, Xia M, Wang M, Wei HS, Zeppenfeld D, et al. Impairment of paravascular clearance pathways in the aging brain. Ann Neurol 2014; 76: 845–61.
Leinonen V, Koivisto AM, Savolainen S, Rummukainen J, Tamminen JN, Tillgren T, et al. Amyloid and tau proteins in cortical brain biopsy and Alzheimer's disease. Ann Neurol 2010; 68: 446–53.
Libard S, Alafuzoff I. Alzheimer's disease neuropathological change and loss of matrix/neuropil in patients with idiopathic Normal Pressure Hydrocephalus, a model of Alzheimer's disease. Acta Neuropathol Commun 2019; 7: 3.
Lindstrom EK, Ringstad G, Mardal KA, Eide PK. Cerebrospinal fluid volumetric net flow rate and direction in idiopathic normal pressure hydrocephalus. NeuroImage Clin 2018; 20: 731–41.
Louveau A, Plog BA, Antila S, Alitalo K, Nedergaard M, Kipnis J. Understanding the functions and relationships of the glymphatic system and meningeal lymphatics. J Clin Invest 2017; 127: 3210–9.
Ma Q, Ineichen BV, Detmar M, Proulx ST. Outflow of cerebrospinal fluid is predominantly through lymphatic vessels and is reduced in aged mice. Nat Commun 2017; 8: 1434.
Marmarou A, Bergsneider M, Klinge P, Relkin N, Black PM. The value of supplemental prognostic tests for the preoperative assessment of idiopathic normal-pressure hydrocephalus. Neurosurgery 2005; 57: S2-17– 28. discussion ii-v.
Marmarou A, Young HF, Aygok GA, Sawauchi S, Tsuji O, Yamamoto T, et al. Diagnosis and management of idiopathic normal-pressure hydrocephalus: a prospective study in 151 patients. J Neurosurg 2005; 102: 987–97.
Mestre H, Tithof J, Du T, Song W, Peng W, Sweeney AM, et al. Flow of cerebrospinal fluid is driven by arterial pulsations and is reduced in hypertension. Nat Commun 2018; 9: 4878.
Mori E, Ishikawa M, Kato T, Kazui H, Miyake H, Miyajima M, et al. Guidelines for management of idiopathic normal pressure hydrocephalus: second edition. Neurol Med Chir(Tokyo) 2012; 52: 775–809.
Nagelhus EA, Ottersen OP. Physiological roles of aquaporin-4 in brain. Physiol Rev 2013; 93: 1543–62.
Nehra AK, McDonald RJ, Bluhm AM, Gunderson TM, Murray DL, Jannetto PJ, et al. Accumulation of gadolinium in human cerebrospinal fluid after gadobutrol-enhanced MR imaging: a prospective observational cohort study. Radiology 2018; 288: 416–23.
Pomeraniec IJ, Bond AE, Lopes MB, Jane JA. Sr., Concurrent Alzheimer's pathology in patients with clinical normal pressure hydrocephalus: correlation of high-volume lumbar puncture results, cortical brain biopsies, and outcomes. J Neurosurg 2016; 124: 382–8.
Qvarlander S, Malm J, Eklund A. CSF dynamic analysis of a predictive pulsatility-based infusion test for normal pressure hydrocephalus. Med Biol Eng Comput 2014; 52: 75–85.
Radbruch A, Haase R, Kieslich PJ, Weberling LD, Kickingereder P, Wick W, et al. No signal intensity increase in the dentate nucleus on unenhanced T1-weighted MR images after more than 20 serial injections of macrocyclic gadolinium-based contrast agents. Radiology 2017; 282: 699–707.
Reeves BC, Karimy JK, Kundishora AJ, Mestre H, Cerci HM, Matouk C, et al. Glymphatic system impairment in Alzheimer's disease and idiopathic normal pressure hydrocephalus. Trends Mol Med 2020; 26: 285–95.
Relkin N, Marmarou A, Klinge P, Bergsneider M, Black PM. Diagnosing idiopathic normal-pressure hydrocephalus. Neurosurgery 2005; 57: S2-4–16. discussion ii-v.
Ringstad G, Eide PK. Cerebrospinal fluid tracer efflux to parasagittal dura in humans. Nat Commun 2020; 11: 354.
Ringstad G, Valnes LM, Dale AM, Pripp AH, Vatnehol SS, Emblem KE, et al. Brain-wide glymphatic enhancement and clearance in humans assessed with MRI. JCI Insight 2018; 3.
Ringstad G, Vatnehol SAS, Eide PK. Glymphatic MRI in idiopathic normal pressure hydrocephalus. Brain 2017; 140: 2691–705.
Rissman RA, Trojanowski JQ, Shaw LM, Aisen PS. Longitudinal plasma amyloid beta as a biomarker of Alzheimer's disease. J Neural Transm 2012; 119: 843–50.
Roman GC, Jackson RE, Fung SH, Zhang YJ, Verma AK. Sleep-disordered breathing and idiopathic normal-pressure hydrocephalus: recent pathophysiological advances. Curr Neurol Neurosci Rep 2019; 19: 39.
Sakono M, Zako T. Amyloid oligomers: formation and toxicity of Abeta oligomers. FEBS J 2010; 277: 1348–58.
Scheltens P, Leys D, Barkhof F, Huglo D, Weinstein HC, Vermersch P, et al. Atrophy of medial temporal lobes on MRI in "probable" Alzheimer's disease and normal ageing: diagnostic value and neuropsychological correlates. J Neurol Neurosurg Psychiatry 1992; 55: 967–72.
Sweeney MD, Zlokovic BV. A lymphatic waste-disposal system implicated in Alzheimer's disease. Nature 2018; 560: 172–4.
Valnes LM, Mitusch SK, Ringstad G, Eide PK, Funke SW, Mardal KA. Apparent diffusion coefficient estimates based on 24 hours

tracer movement support glymphatic transport in human cerebral cortex. Sci Rep 2020; 10: 9176.

Vanneste J, Augustijn P, Davies GA, Dirven C, Tan WF. Normal-pressure hydrocephalus. Is cisternography still useful in selecting patients for a shunt? Arch Neurol 1992; 49: 366–70.

Virhammar J, Laurell K, Cesarini KG, Larsson EM. The callosal angle measured on MRI as a predictor of outcome in idiopathic normal-pressure hydrocephalus. J Neurosurg 2014; 120: 178–84.

Xie L, Kang H, Xu Q, Chen MJ, Liao Y, Thiyagarajan M, et al. Sleep drives metabolite clearance from the adult brain. Science 2013; 342: 373–7.

Yamada S, Ishikawa M, Yamamoto K. Optimal diagnostic indices for idiopathic normal pressure hydrocephalus based on the 3D quantitative volumetric analysis for the cerebral ventricle and subarachnoid space. Am J Neuroradiol 2015; 36: 2262–9.

Zhou Y, Cai J, Zhang W, Gong X, Yan S, Zhang K, et al. Impairment of the glymphatic pathway and putative meningeal lymphatic vessels in the aging human. Ann Neurol 2020; 87: 357–69.

Zou W, Pu T, Feng W, Lu M, Zheng Y, Du R, et al. Blocking meningeal lymphatic drainage aggravates Parkinson's disease-like pathology in mice overexpressing mutated alpha-synuclein. Transl Neurodegener 2019, doi: 10.1007/s00234-020-025194.